VNU Journal of Science: Mathematics - Physics

Journal homepage: https://js.vnu.edu.vn/MaP

Original Article

Nonlinear Vibration of Nanocomposite Multilayer Perovskite Solar Cell in Thermal Environment

Vu Dinh Khoe[1], Pham Minh Vuong[2], Nguyen Van Thanh[1,3], Tran Quoc Quan[1,*], Nguyen Dinh Duc[1]

[1]*VNU University of Engineering and Technology, 144 Xuan Thuy, Cau Giay, Hanoi, Vietnam*

[2]*University of Civil Engineering, 55 Giai Phong, Hai Ba Trung, Hanoi, Vietnam*

[3]*Military Academy of Logistics, Ngoc Thuy, Lon Bien, Hanoi, Vietnam*

Received 19 August 2021
Revised 29 August 2021; Accepted 30 August 2021

Abstract: In this work we investigated the nonlinear vibration of nanocomposite multilayer perovskite solar cell (NMPSC) subjected to the combination of mechanical and thermal loadings. The model of organic solar cell is assumed to consist seven functional layers: Au, Spiro-OMeTAD, PEDOT:PSS, Graphene oxide, $MAPbI_3$, TiO_2 and IOT, and glass substrate. The governing equations are established basing on the classical plate theory taking into account the effect of elastic foundations and initial imperfection. Four edges of the NMPSC are assumed to be supported immovably in a transverse plane. The relationship between deflection amplitude and time as well as the expression of natural frequency of NMPSC are obtained by using the Galerkin and Runge – Kutta methods. The numerical results showed that the nonlinear dynamic response and the natural frequency of NMPSC have been strongly influenced by the geometrical and material parameters, initial imperfection, temperature increment and elastic foundations.

Keywords: Perovskite solar cell; nonlinear vibration; elastic foundations; initial imperfection; thermal environment.

1. Introduction

Perovskite solar cells included a perovskite structured compound have shown advantages in the high performance parameters and low production costs. Studies on the synthesis, properties and behaviours of perovskite solar cell structures have received considerable attention from scientists

* Corresponding author.
E-mail address: quantq1505@gmail.com

https//doi.org/10.25073/2588-1124/vnumap.4671

around the world. Wu et al., [1] introduced an inter-layer of phytic acid sodium between the NiO_x hole transporting layer and the perovskite absorption layer to enhance the quality and coverage of perovskite solar cells. Ding et al., [2] adopted metal bis(trifluoromethanesulfonyl)imide to modify mesoporous TiO_2 electron transport layer of perovskite solar cells and performed electrochemical impedance spectroscopy, photoluminescence spectrum, space-charge limited current, and X-ray photoelectron spectroscopy measurements to investigate the modification mechanisms. Further, Sfyri et al., [3] made solid state hybrid perovskite solar cells by employing a layer structure of nanoparticulate titania, organometal halide perovskite and spiro-MeOTAD as hole transporter. Xu et al., [4] investigated the effect of antisolvent treatment on PbI_2 films for high performance carbon-based perovskite solar cells. It is found that the diethyl ether treated corresponding perovskite film has smoother surface morphology and enhanced carrier transport property compared with the pristine perovskite film and the film treated by the chlorobenzene. Wang et al., [5] fabricated a series of perovskite-based solar cells wherein a compact layer of TiO_2 of varying thickness (0–390 nm) was introduced by spray pyrolysis deposition between fluorine-doped tin oxide electrode and TiO_2 nanoparticle layer. In 2020, Dat et al., [6] carried out the nonlinear stability of nanocomposite multilayer organic solar cell subjected to axial compressive loads in which the model of organic solar cell is assumed to consist four functional layers as Al, P3HT:PCBM, PEDOT:PSS and IOT, and glass substrate. By analyzing the types and mechanism of inorganic perovskite film defects, the influence of inorganic perovskite film preparation technique on crystallization in recent years is reviewed, passivation strategies for different kinds of additives are discussed in combination with Lewis acid base theory, and interface engineering on both sides of the perovskite film is summarized in the work of Han et al., [7].

Plate, shell and panel are basic structures used in engineering and industry. These structures play an important role as main supporting components in all kind of structures in machinery, civil engineering, ship building, flight vehicle manufacturing, etc. The vibration of composite plate and shell is the first and most important problem in optimal design. Li et al., [8] presented full-scale modeling and nonlinear finite element analysis for large amplitude vibration of sandwich plates with functionally graded auxetic 3D lattice core. Based on the threedimensional theory of elasticity, Liew and Alibeigloo [9] investigated the buckling and free vibration studies of functionally graded carbon nanotube reinforced composite cylindrical panel with different patterns of carbon nanotube distribution. Besides, Jafari and Kiani [10] dealt with the free vibration response of composite plates which are reinforced with graphene plates using the Halpin Tsai model which captures the dimensions of the reinforcement. Phuc et al., [11] introduced Shi's high-order shear deformation theory to compute the free vibration of the cracked functionally graded material plates according to the power law resting on Pasternak elastic foundations; Quyen et al., [12] studied the nonlinear free and forced vibration of sandwich cylindrical panel on visco-Pasternak foundations in thermal environment subjected to blast load. Recently, Teng and Wang [13] investigated nonlinear forced vibration of graphene platelet reinforced metal foam rectangular plates using the von Kármán nonlinear plate theory. Askari et al., [14] proposed a mathematical method to study fluid-coupled vibration of axisymmetric plate structures with asymmetries due to either imperfection or practical reasons, e.g. the weight reduction of structure, natural frequency shifting, and accessibility. Vinyas et al., [15] dealt with evaluating the frequency response of functionally graded carbon nanotube reinforced magneto-electro-elastic plates subjected to open and closed electro-magnetic circuit conditions. Further, Avey et al., [16] investigated the nonlinear vibration of moderately thick multilayer shelltype structural elements with double curvature consisting of carbon nanotube patterned layers within different shell theories. Permoon and Farsadi [17] studied the natural frequencies and damping behavior of three-layer sandwich plates with viscoelastic core modelled with fractional theory.

This paper introduces analytical solutions for the nonlinear vibration of an imperfect nanocomposite multilayer perovskite solar cell (NMPSC). The perovskite solar cell is comprised of seven functional layers of isotropic materials. The NMPSC is assumed to be supported by elastic foundations and subjected to the combination of mechanical and thermal loadings. The governing equations are established basing on the classical plate theory and solved by the Galerkin and Runge-Kutta methods.

2. Problem Statement

In this study, NMPSC which consists of seven functional layers: Au, Spiro-OMeTAD, PEDOT:PSS, graphene oxide (GO), $MAPbI_3$, TiO_2 and ITO-coated glass with length a, width b and total thickness h is considered as Figure 1. Each layer of NMPSC is assumed to be isotropic material and the effective properties of layers such as Young's modulus E, Poisson's ratio ν, the mass density ρ and the thermal expansion coefficients α are shown in Table 1. A Cartesian coordinate system (x, y, z) is established in which (x, y) plane on the middle surface of the NMPSC and z on thickness direction $(-h/2 \le z \le h/2)$.

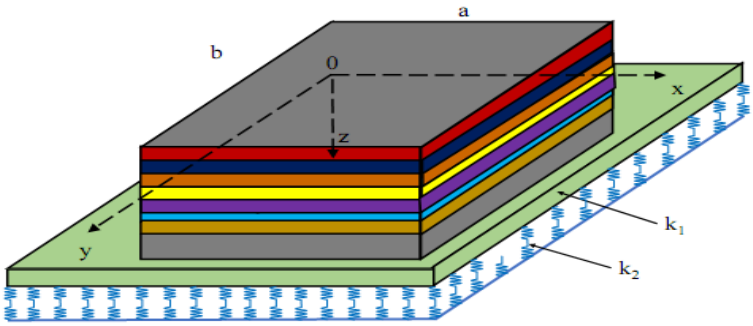

Figure 1. Modeling of the NMPSC on elastic foundations.

The NMPSC is assumed to rest on elastic foundations of Pasternak-type model. The interaction between the NMPSC and elastic foundations is expressed as

$$q_e = k_1 w - k_2 \Delta w, \tag{1}$$

in which w is the deflection of the NMPSC, k_1 is Winkler foundation modulus and k_2 is the shear layer foundation stiffness of Pasternak model.

Table 1. The initial thickness and mechanical properties of seven functional layers and ITO-coated glass substrate in NMPSC.

Layer	h	$E(GPa)$	ν	$\rho(kg/m^3)$	$\alpha(\times 10^{-6}\,1/{}^0C)$
Au	100 nm	77.2	0.42	19300	14
Spiro-OMeTAD	100 nm	68	0.33	1060	28
PEDOT:PSS	50 nm	2.3	0.4	1000	70
Graphene oxide (GO)	1.45 nm	444.8	0.27	1800	-67
$MAPbI_3$	450 nm	12.8	0.33	4100	157
TiO_2	170 nm	230	0.27	4260	8.4
ITO	120 nm	116	0.35	7140	7.2
Glass Substrate	550 µm	69	0.23	2400	9

3. Basic Equations

3.1. Motion Equations System

In this study, the classical plate theory [18, 19] is used to establish the basic equations and investigate the nonlinear vibration of the NMPSC on elastic foundations. The strain components at a distance z from the mid-plane and on the middle surface of the NMPSC taking into account von Kárman nonlinear terms can be expressed as:

$$\begin{pmatrix} \varepsilon_x \\ \varepsilon_y \\ \gamma_{xy} \end{pmatrix} = \begin{pmatrix} \varepsilon_x^0 \\ \varepsilon_y^0 \\ \gamma_{xy}^0 \end{pmatrix} - z \begin{pmatrix} w_{,xx} \\ w_{,yy} \\ 2w_{,xy} \end{pmatrix}, \begin{pmatrix} \varepsilon_x^0 \\ \varepsilon_y^0 \\ \gamma_{xy}^0 \end{pmatrix} = \begin{pmatrix} u_{,x} + \frac{1}{2} w_{,x}^2 \\ v_{,\mathrm{y}} + \frac{1}{2} w_{,\mathrm{y}}^2 \\ u_{,x} + v_{,\mathrm{y}} + \frac{1}{2} w_{,x} w_{,\mathrm{y}} \end{pmatrix}, \tag{2}$$

where u, v are the displacement components along the x, y directions, respectively.

The relationships between stress and strain for the *kth* layer of the NMPSC are determined by Hooke's Law as

$$\begin{pmatrix} \sigma_x \\ \sigma_y \\ \sigma_{xy} \end{pmatrix}_k = \begin{pmatrix} Q_{11}^{'} & Q_{12}^{'} & Q_{16}^{'} \\ Q_{12}^{'} & Q_{22}^{'} & Q_{26}^{'} \\ Q_{16}^{'} & Q_{26}^{'} & Q_{66}^{'} \end{pmatrix}_k \begin{pmatrix} \varepsilon_x - \alpha \Delta T \\ \varepsilon_y - \alpha \Delta T \\ \gamma_{xy} \end{pmatrix}_k, \tag{3}$$

in which stiffness coefficients of the *k*th layer of the NMPSC are defined as

$$\left(Q_{11}^{'}\right)_k = \frac{E_k}{1-\nu_k^2}, \left(Q_{12}^{'}\right)_k = \frac{\nu_k E_k}{1-\nu_k^2}, \left(Q_{22}^{'}\right)_k = \left(Q_{11}^{'}\right)_k, \left(Q_{66}^{'}\right)_k = \frac{E_k}{2\left(1+\nu_k\right)}. \tag{4}$$

The force and moment resultants of the NMPSC are expressed as

$$\begin{aligned} N_x &= Q_1 \varepsilon_x^0 + Q_2 \varepsilon_y^0 + Q_3 k_x + Q_4 k_y - Q_5 \Delta T, \\ N_y &= Q_2 \varepsilon_x^0 + Q_1 \varepsilon_y^0 + Q_4 k_x + Q_3 k_y - Q_5 \Delta T, \\ N_{xy} &= Q_6 \gamma_{xy}^0 + Q_7 k_{xy}, \\ M_x &= Q_3 \varepsilon_x^0 + Q_4 \varepsilon_y^0 + Q_8 k_x + Q_9 k_y - Q_{10} \Delta T, \\ M_y &= Q_4 \varepsilon_x^0 + Q_3 \varepsilon_y^0 + Q_9 k_x + Q_8 k_y - Q_{10} \Delta T, \\ M_{xy} &= Q_{11} \gamma_{xy}^0 + Q_{12} k_{xy}, \end{aligned} \tag{5}$$

where the details of coefficients Q_i $(i = \overline{1,12})$ are given in Appendix A.

The geometrical compatibility equation for an imperfect NMPSC is written as [18, 19]

$$\frac{\partial^2 \varepsilon_x^0}{\partial y^2} + \frac{\partial^2 \varepsilon_y^0}{\partial x^2} - \frac{\partial^2 \gamma_{xy}^0}{\partial x \partial y} = \left(\frac{\partial^2 w}{\partial x \partial y}\right)^2 - \frac{\partial^2 w}{\partial x^2}\frac{\partial^2 w}{\partial y^2} + 2\frac{\partial^2 w}{\partial x \partial y}\frac{\partial^2 w^*}{\partial x \partial y} - \frac{\partial^2 w}{\partial x^2}\frac{\partial^2 w^*}{\partial y^2} - \frac{\partial^2 w}{\partial y^2}\frac{\partial^2 w^*}{\partial x^2}. \tag{6}$$

Based on the classical plate theory, the nonlinear motion equations of the NMPSC are expressed as [18, 19].

$$N_{x,x} + N_{xy,y} = 0, \tag{7a}$$

$$N_{xy,x} + N_{y,y} = 0, \tag{7b}$$

$$M_{x,xx} + 2M_{xy,xy} + M_{y,yy} + N_x w_{,xx} + 2N_{xy} w_{,xy} + N_y w_{,yy} + q + k_1 w - k_2 \left(w_{,xx} + w_{,yy} \right) = \rho_1 w_{,tt}, \tag{7c}$$

where

$$\rho_1 = \sum_{k=1}^{8} \int_{z_k}^{z_{k+1}} \rho_k dz. \tag{8}$$

The Airy's stress function $f\left(x, y, t\right)$ is introduced as

$$N_x = \frac{\partial^2 f}{\partial y^2}, N_y = \frac{\partial^2 f}{\partial x^2}, N_x = \frac{\partial^2 f}{\partial x \partial y}. \tag{9}$$

Boundary conditions and analytical solutions are as following.

Four edges of the imperfect NMPSC are assumed to be simply supported and immovable in xy plane. The boundary conditions are

$$\begin{aligned} &w = N_{xy} = M_x = 0, N_x = N_x^0 \;\; at \;\; x = 0, a, \\ &w = N_{xy} = M_y = 0, \; N_y = N_y^0 \;\; at \;\; y = 0, b. \end{aligned} \tag{10}$$

Based on the boundary conditions in Eq. (10), the deflection w and initial imperfection w^* are assumed to be in approximate forms as [18, 19]

$$\left(w, w^* \right) = \left(W, \mu h \right) \sin \lambda x \sin \beta y, \tag{11}$$

in which $\lambda = m\pi / a, \; \beta = n\pi / b;$ m, n are odd natural numbers representing the number of half waves in the x and y directions, respectively; $W(t)$ is the time dependent amplitudes and μ is imperfection parameter of the NMPSC.

Substituting Eq. (11) into the compatibility equation (6) and balancing the coefficients of the two sides in the resulting equation, we can obtain the stress function f as

$$f = C_1 \cos 2\lambda x + C_2 \cos 2\beta y + C_3 \sin \lambda x \sin \beta y + \frac{1}{2} N_x^0 y^2 + \frac{1}{2} N_y^0 x^2, \tag{12}$$

with

$$\begin{aligned} C_1 &= \frac{\beta^2 W \left(W + 2\mu h \right)}{32 P_5 \lambda^2}, \\ C_2 &= \frac{\lambda^2 W \left(W + 2\mu h \right)}{32 P_5 \beta^2}, \\ C_3 &= \frac{-W(P_7 \lambda^4 + P_8 \lambda^2 \beta^2 + P_7 \beta^4)}{P_5 \lambda^4 + P_6 \lambda^2 \beta^2 + P_5 \beta^4}. \end{aligned} \tag{13}$$

3.2. Nonlinear Vibration Analysis

Replacing Eqs. (11) and (12) into Eqs. (7) then applying the Bubnov – Galerkin method yields the following:

$$\begin{aligned} &H_1W + H_2\left(W+\mu h\right) + H_3W\left(W+\mu h\right) + H_4W\left(W+2\mu h\right) + H_5W\left(W+\mu h\right)\left(W+2\mu h\right) \\ &+H_6q - \left(N_{x0}\lambda^2 + N_{y0}\beta^2\right)\frac{1}{4}\left(W+\mu h\right) = \frac{1}{4}\rho_1\frac{\delta^2W}{\delta t^2}, \end{aligned} \tag{14}$$

where the details of coefficients H_i $(i=\overline{1,6})$ are given in Appendix B.

The condition expressing the immovability on the four edges of NMPSC is satisfied in an average sense as

$$\int_0^b\int_0^a \frac{\partial u}{\partial x}dxdy = 0,\ \int_0^a\int_0^b \frac{\partial v}{\partial y}dxdy = 0. \tag{15}$$

We can obtain the expressions of the derivative of displacement components as

$$\begin{aligned} \frac{\partial u}{\partial x} &= \frac{Q_1}{Q_1^2-Q_2^2}f_{,\mathrm{yy}} - \frac{Q_2}{Q_1^2-Q_2^2}f_{,\mathrm{xx}} + \frac{Q_1Q_3-Q_2Q_4}{Q_1^2-Q_2^2}\mathrm{w}_{,xx} \\ &+\frac{Q_1Q_4-Q_2Q_3}{Q_1^2-Q_2^2}\mathrm{w}_{,yy} - \frac{-Q_1Q_5+Q_2Q_5}{Q_1^2-Q_2^2}\Delta T - \frac{\mathrm{w}_{,x}^2}{2} - \mathrm{w}_{,x}\mathrm{w}_{,x}^*, \\ \frac{\partial v}{\partial y} &= -\frac{Q_2}{Q_1^2-Q_2^2}f_{,\mathrm{yy}} + \frac{Q_1}{Q_1^2-Q_2^2}f_{,\mathrm{xx}} + \frac{Q_1Q_4-Q_2Q_3}{Q_1^2-Q_2^2}\mathrm{w}_{,xx} \\ &+\frac{Q_1Q_3-Q_2Q_4}{Q_1^2-Q_2^2}\mathrm{w}_{,yy} - \frac{-Q_1Q_5+Q_2Q_5}{Q_1^2-Q_2^2}\Delta T - \frac{\mathrm{w}_{,y}^2}{2} - \mathrm{w}_{,y}\mathrm{w}_{,y}^*. \end{aligned} \tag{16}$$

The fictitious compressive edge loads at immovable edges are obtained as

$$\begin{aligned} N_{x0} &= G_1W + G_2\mathrm{W}\left(W+2uh\right) - G_3\Delta T, \\ N_{y0} &= G_4W + G_5\mathrm{W}\left(W+2uh\right) - G_3\Delta T, \end{aligned} \tag{17}$$

where the details of coefficients G_i $(i=\overline{1,5})$ are given in Appendix C.

Substituting Eq. (17) into Eqs. (14), Eq. (14) becomes

$$\begin{aligned} &K_1W + K_2\left(W+\mu h\right) + K_3W\left(W+\mu h\right) + K_4\mathrm{W}\left(W+2\mu h\right) \\ &+K_5W\left(W+2\mu h\right)\left(W+\mu h\right) + K_6q = \frac{1}{4}\rho_1\frac{\delta^2W}{\delta t^2}, \end{aligned} \tag{18}$$

in which

$$\begin{aligned} &K_1 = H_1,\ K_2 = \frac{1}{4}\left(P_3\lambda^4 + P_4\lambda^2\beta^2 + P_3\beta^4\right) + \frac{1}{4}G_3\Delta T(\beta^2+\lambda^2), \\ &K_3 = H_3 - \frac{1}{4}\left(G_1\lambda^2 + G_4\beta^2\right), K_4 = H_4, K_5 = H_5 - \frac{1}{4}\left(G_2\lambda^2 + G_5\beta^2\right), K_6 = H_6. \end{aligned} \tag{19}$$

Eq. (18) is used to consider the nonlinear vibration characteristics of imperfect NMPSC in thermal environments in which the nonlinear dynamic response is obtained by using Runge – Kutta method with the initial conditions as $W(0)=0,\ \dfrac{dW}{dt}(0)=0$.

From Eq. (18), the natural frequencies of a perfect NMPSC can be calculated by the expression as

$$\omega_{mn} = \sqrt{\frac{-4(K_1 + K_2)}{\rho_1}} \tag{20}$$

4. Results and Discussion

Table 2 shows the effect of the length to width ratio a/b, modes of vibration (m,n) and elastic foundations with two coefficients $k_1\,(GPa/m)$, $k_2\,(GPa.m)$ on the natural frequency $(\times 10^6\ s^{-1})$ of the NMPSC. As can be observed, the value of the natural frequency of the NMPSC increases significantly when the values of modes (m,n) increase. The results from Table 2 also illustrate that the natural frequency of the NMPSC with the higher elastic foundations coefficients is higher than one of the NMPSC with lower elastic foundations coefficients. The reason is that the elastic foundations enhance the stiffness of the sandwich plate. Besides, the natural frequency becomes larger as the ratio a/b increases.

Table 2. Effects of a/b ratio, elastic foundations and vibration modes (m,n) on the natural frequencies of the NMPSC.

a/b	(k_1, k_2)	(m,n)			
		(1,1)	(1,3)	(3,1)	(3,3)
0.5	(1, 0.02)	0.24834	0.39900	0.67243	0.74158
1	(1, 0.02)	0.31343	0.69916	0.69916	0.93832
2	(1, 0.02)	0.49455	1.34716	0.79722	1.48653
0.5	(1.5, 0.04)	0.35123	0.56480	0.95198	1.04984
1	(1.5, 0.04)	0.44353	0.98981	0.98981	1.32817
2	(1.5, 0.04)	0.70016	1.90532	1.12853	2.10182

The effects of temperature increment $\Delta T(=0,100\,K,200\,K,500\,K)$ and the length to thickness ratio $a/h(=80,100,120)$ on the natural frequency $(\times 10^6\ s^{-1})$ of the NMPSC are given in Table 3. As expected, the value of natural oscillation frequency decreases slowly when the value of temperature increment increases. The results also confirm that the a/h ratio reduces the stiffness of the NMPSC, the natural frequency decreases as the a/h ratio increases.

Table 3. Effects of a/h ratio and temperature increment on the natural frequencies of the NMPSC.

a/h	$\Delta T\,(K)$			
	0	100	200	500
80	0.39172	0.39128	0.39085	0.38954
100	0.31339	0.31304	0.31269	0.31165
120	0.26119	0.26090	0.26061	0.25974

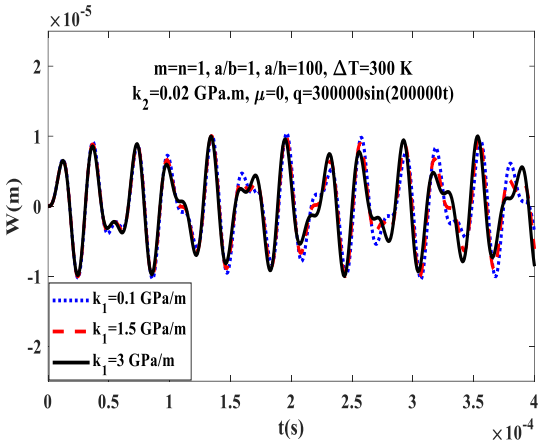

Figure 2. Effect of Winkler foundation on the dynamic response of NMPSC.

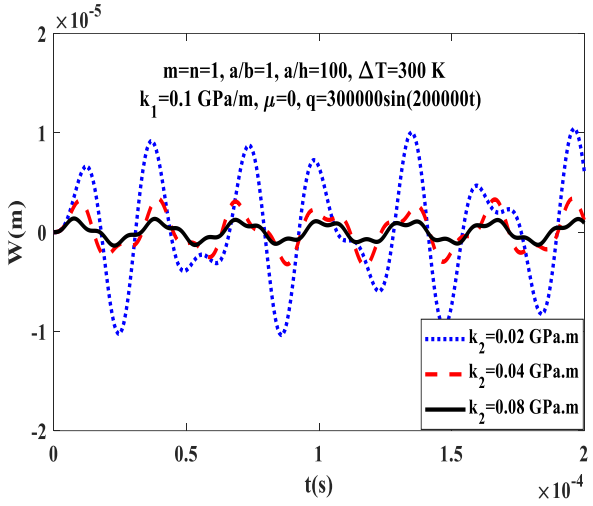

Figure 3. Effect of Pasternak foundation on the dynamic response of NMPSC.

Figures 2 and 3 indicate the effect of elastic foundations with two stiffness coefficients on the relationship between deflection amplitude and time of the imperfect NMPSC, respectively. As can be seen, elastic foundations have positive influences on the dynamic response of the NMPSC. Specifically, the deflection amplitude decreases significantly with the increase of two modulus. Moreover, the effect of Pasternak modulus on the dynamic response of the NMPSC is stronger than the one of Winkler foundation.

Figures 4 and 5 show the *a/b* and *a/h* ratios effect of the nonlinear dynamic response of the NMPSC on elastic foundations subjected to mechanical loading and temperature change, respectively. There values of a/b ratio and three values of a/h ratio are considered. As can be observed, an increase of a/b ratio or a decrease of a/h ratio leads to a decrease of the deflection amplitude of the NMPSC. This is because the stiffness of the NMPSC reduces as the a/b ratio decreases or the a/h ratio increases.

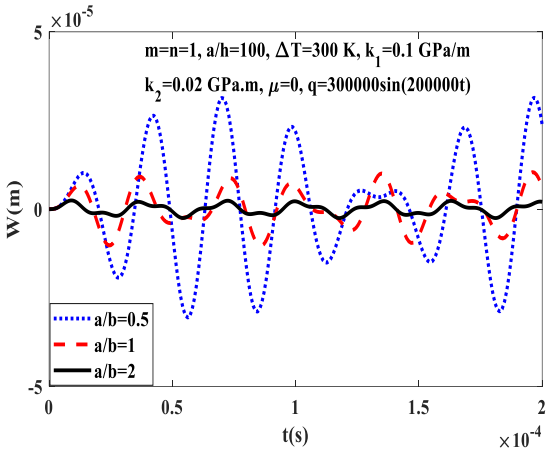

Figure 4. Effect of *a/b* ratio on the dynamic response of NMPSC.

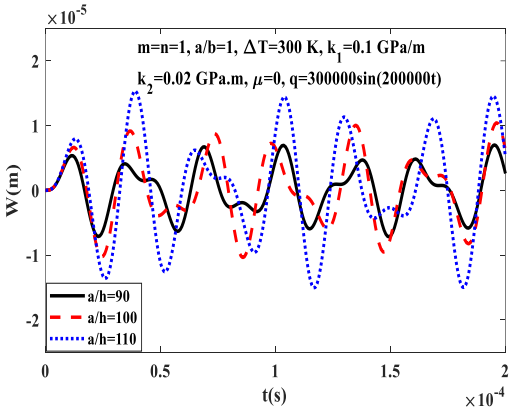

Figure 5. Effect of *a/h* ratio on the dynamic response of NMPSC.

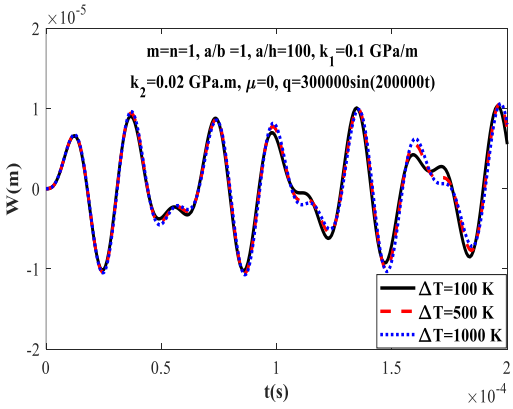

Figure 6. Effect of temperature increment on the dynamic response of NMPSC.

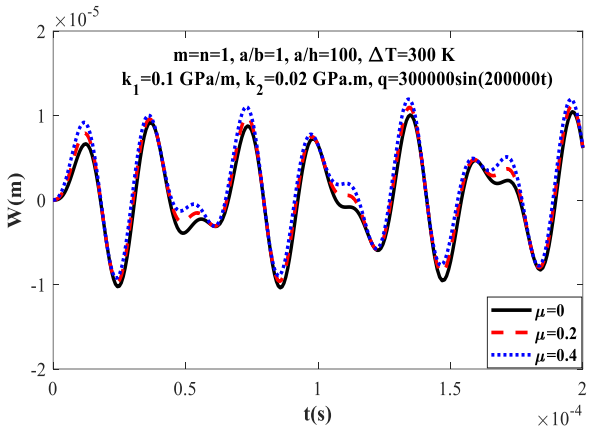

Figure 7. Effect of initial imperfection on the dynamic response of NMPSC.

Figure 6 presents the effect of temperature increment ΔT on the nonlinear dynamic response of NMPSC on elastic foundations with immovable edges subjected to the combination of mechanical and thermal loadings. The geometrical parameters of the NMPSC are taken to be $a/b=1$, $a/h=100$. As can be observed, the temperature increment has the negative influence on the nonlinear dynamic response of the NMPSC. The deflection amplitude of the NMPSC increases significantly as the temperature increment increases.

Figure 7 illustrates the effect of inital imperfection with coefficient μ on the nonlinear dynamic response of the NMPSC. It is easy to see that the deflection amplitude is very sensitive with the change of the initial imperfection coefficient. The deflection amplitude of the NMPSC increases considerably as the initial imperfection coefficient increases.

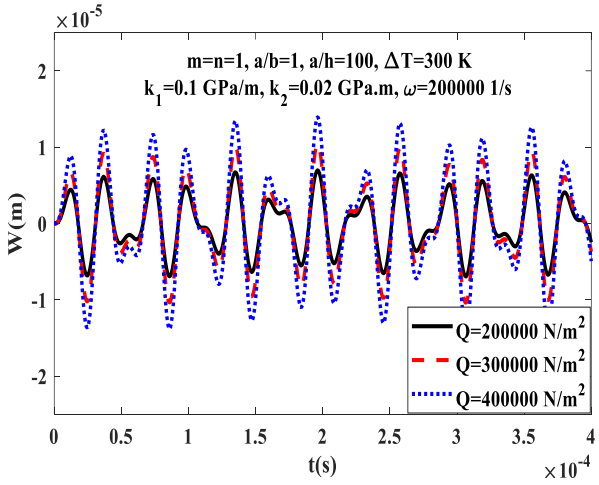

Figure 8. Effect of exciting force amplitude on the dynamic response of NMPSC.

Figure 8 shows the effect of the exciting force amplitude on nonlinear dynamic response of NMPSC in the cases of $Q=200000,\ 300000,\ 400000\ N/m^2$. Obviously, the deflection amplitude of NMPSC increases when the exciting force amplitude increases.

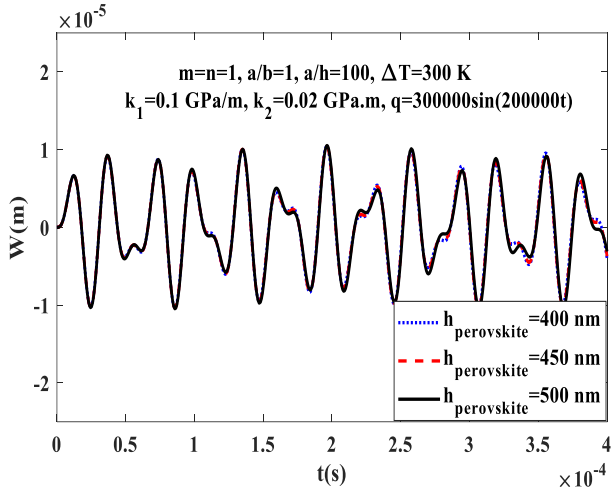

Figure 9. Effect of the thickness of perovskite layer on the dynamic response of NMPSC.

Figure 9 indicates the effect of the thickness of perovskite ($MAPbI_3$) layer $h_{perovskite}$ on the nonlinear dynamic response of the NMPSC subjected to the combination of mechanical and thermal loadings. As can be seen, the changes are very small. The deflection amplitude of the NMPSC increases lightly as $h_{perovskite}$ increases. The reason is that the structural stiffness of NMPSC increases with the increase of the thickness of perovskite layer.

5. Conclusions

This work dealt with the nonlinear vibration of imperfect NMPSC under the mechanical load in thermal environment. The natural frequency and the dynamic response of the NMPSC are obtained by using the Galerkin and Runge – Kutta methods. There are some conclusions obtained from numerical results:

- The increase of foundation stiffness k_1 and k_2 results in the increase of the natural frequency and the decrease of the deflection amplitude of the NMPSC.
- The natural frequency decreases and the deflection amplitude increases when the temperature increment rises.
- An increase of the exciting force amplitude leads to an increase of the deflection amplitude of the NMPSC.
- The deflection amplitude of the NMPSC is negative and the deflection amplitude increases as the initial imperfection coefficient is increased.
- The geometrical parameters have strong effect on the nonlinear vibration of the NMPSC.

Acknowledgments

This research is funded by Vietnam National Foundation for Science and Technology Development (NAFOSTED) under grant number 107.02-2019.01.

References

[1] C. Wu, Y. Huang, S. Wang, X. Miao, R. Ma, C. Wang, Phytate Modifies The Hole Transport Layer and Assists in Blade Coating to Prepare Efficient Perovskite Solar Cells, Solar Energy, Vol. 203, 2020, pp. 25-31, https://doi.org/10.1016/j.solener.2020.03.086.

[2] B. Ding, X. Zhao, S. Wang, X. Shan, Z. Chen, Z. Deng, et al, Mechanism of Improving The Performance of Perovskite Solar Cells Through Alkali Metal Bis(trifluoromethanesulfonyl)imide Modifying Mesoporous Titania Electron Transport Layer, Journal of Power Sources, Vol. 484, 2021, pp. 229275, https://doi.org/10.1016/j.jpowsour.2020.229275.

[3] G. Sfyri, C. V. Kumar, D. Raptis, V. Dracopoulos, P. Lianos, Study of Perovskite Solar Cells Synthesized under Ambient Conditions and of The Performance of Small Cell Modules, Solar Energy Materials and Solar Cells, Vol. 134, 2015, pp. 60-63, https://doi.org/10.1016/j.solmat.2014.11.034.

[4] T. Xu, K. Zou, X. Sun, Z. Wan, H. Tang, Y. Zhang, et al, Effect of Antisolvent Treatment on PbI2 Films for High Performance Carbon-based Perovskite Solar Cells, Materials Letters, Vol. 275, 2020, pp. 128157, https://doi.org/10.1016/j.matlet.2020.128157.

[5] X. Wang, Y. Fang, L. He, Q. Wang, T. Wu, Influence of Compact TiO2 Layer on The Photovoltaic Characteristics of The Organometal Halide Perovskite-based Solar Cells, Materials Science in Semiconductor Process, Vol. 27, 2014, pp. 569-576, https://doi.org/10.1016/j.mssp.2014.07.039.

[6] N. D. Dat, V. M. Anh, T. Q. Quan, P. T. Duc, N. D. Duc, Nonlinear Stability and Optimization of Thin Nanocomposite Multilayer Organic Solar Cell Using Bees Algorithm, Thin-Walled Structures, Vol. 149, 2020, pp. 106520. https://doi.org/10.1016/j.tws.2019.106520.

[7] S. Han, H. Zhang, R. Wang, Q. He, Research Progress of Absorber Film of Inorganic Perovskite Solar Cells: Fabrication Techniques and Additive Engineering in Defect Passivation, Materials Science in Semiconductor Process, Vol. 127, 2021, pp. 105666, https://doi.org/10.1016/j.mssp.2021.105666.

[8] C. Li, H. S. Shen, H. Wang, Z. Yu, Large Amplitude Vibration of Sandwich Plates with Functionally Graded Auxetic 3D Lattice Core, International Journal of Mechanical Sciences, Vol. 174, 2020, pp. 105472, https://doi.org/10.1016/j.ijmecsci.2020.105472.

[9] K. M. Liew, A. Alibeigloo, Predicting Bucking and Vibration Behaviors of Functionally Graded Carbon Nanotube Reinforced Composite Cylindrical Panels with Three-dimensional Flexibilities, Composite Structures, Vol. 256, 2021, pp. 113039, https://doi.org/10.1016/j.compstruct.2020.113039.

[10] P. Jafari, Y. Kiani, Free Vibration of Functionally Graded Graphene Platelet Reinforced Plates: A Quasi 3D Shear and Normal Deformable Plate Model, Composite Structures, Vol. 275, 2021, pp. 114409, https://doi.org/10.1016/j.compstruct.2021.114409.

[11] P. M. Phuc, D. T. Manh, N. D. Duc, Free Vibration of Cracked FGM Plates with Variable Thickness Resting on Elastic Foundations, Thin-Walled Structures, Vol. 161, 2021, pp. 107425, https://doi.org/10.1016/j.tws.2020.107425.

[12] N. V. Quyen, N. V. Thanh, T.Q. Quan, N. D. Duc, Nonlinear Forced Vibration of Sandwich Cylindrical Panel with Negative Poisson's Ratio Auxetic Honeycombs Core and CNTRC Face Sheets, Thin-Walled Structures, Vol. 162, 2021, pp. 107571, https://doi.org/10.1016/j.tws.2021.107571.

[13] M. W. Teng, Y. Q. Wang, Nonlinear Forced Vibration of Simply Supported Functionally Graded Porous Nanocomposite Thin Plates Reinforced with Graphene Platelets, Thin-Walled Structures, Vol. 164, 2021, pp. 107799, https://doi.org/10.1016/j.tws.2021.107799.

[14] E. Askari, K. H. Jeong, K. H. Ahn, M. Amabili, A Mathematical Approach to Study Fluid-coupled Vibration of Eccentric Annular Plates, Journal of Fluids and Structures, Vol. 98, 2020, pp. 103129, https://doi.org/10.1016/j.jfluidstructs.2020.103129.

[15] M. Vinyas, D. Harursampath, S. C. Kattimani, On Vibration Analysis of Functionally Graded Carbon Nanotube Reinforced Magneto-electro-elastic Plates with Different Electro-magnetic Conditions Using Higher Order Finite Element Methods, Defence Technology, Vol. 17, 2021, pp. 287-303, https://doi.org/10.1016/j.dt.2020.03.012.

[16] M. Avey, N. Fantuzzi, A. H. Sofiyev, N. Kuruoglu, Nonlinear Vibration of Multilayer Shell-type Structural Elements with Double Curvature Consisting of CNT Patterned Layers within Different Theories, Composite Structures, Vol. 275, 2021, pp. 114401, https://doi.org/10.1016/j.compstruct.2021.114401.

[17] M. R. Permoon, T. Farsadi, Free Vibration of Three-layer Sandwich Plate with Viscoelastic Core Modelled with Fractional Theory, Mechanics Research Communications, Vol. 116, 2021, pp. 103766, https://doi.org/10.1016/j.mechrescom.2021.103766.

[18] J. N. Reddy, Mechanics of Laminated Composite Plates and Shells: Theory and Analysis, Boca Raton: CRC Press, Florida, 2004.

[19] N. D. Duc, T. Q. Quan, P. H. Cong, Nonlinear Vibration of Auxetic Plates and Shells, Vietnam National University Press, Hanoi, 2021.

Appendixes

Appendix A

$$Q_1=\sum_{k=1}^{8}\int_{z_k}^{z_{k+1}}\frac{E_k}{1-\upsilon_k^2}dz,\ \mathrm{Q}_2=\sum_{k=1}^{8}\int_{z_k}^{z_{k+1}}\frac{E_k\upsilon_k}{1-\upsilon_k^2}dz,\ \mathrm{Q}_3=\sum_{k=1}^{8}\int_{z_k}^{z_{k+1}}\frac{E_k}{1-\upsilon_k^2}zdz,\ \mathrm{Q}_4=\sum_{k=1}^{8}\int_{z_k}^{z_{k+1}}\frac{E_k\upsilon_k}{1-\upsilon_k^2}zdz,$$

$$Q_5=\sum_{k=1}^{8}\int_{z_k}^{z_{k+1}}\frac{E_k\alpha_k}{1-\upsilon_k}dz,\ \mathrm{Q}_6=\sum_{k=1}^{8}\frac{1}{2}\int_{z_k}^{z_{k+1}}\frac{E_k}{1+\upsilon_k}dz,\ \mathrm{Q}_7=\sum_{k=1}^{8}\int_{z_k}^{z_{k+1}}\frac{E_k}{1+\upsilon_k}zdz,$$

$$Q_8=\sum_{k=1}^{8}\int_{z_k}^{z_{k+1}}\frac{E_k}{1-\upsilon_k^2}z^2dz,\ \mathrm{Q}_9=\sum_{k=1}^{8}\int_{z_k}^{z_{k+1}}\frac{E_k\upsilon_k}{1-\upsilon_k^2}z^2dz,\ \mathrm{Q}_{10}=\sum_{k=1}^{8}\int_{z_k}^{z_{k+1}}\frac{E_k\alpha_k}{1-\upsilon_k}zdz,$$

$$Q_{11}=\sum_{k=1}^{8}\frac{1}{2}\int_{z_k}^{z_{k+1}}\frac{E_k}{1+\upsilon_k}zdz,\ \mathrm{Q}_{12}=\sum_{k=1}^{8}\int_{z_k}^{z_{k+1}}\frac{E_k}{1+\upsilon_k}z^2dz.$$

Appendix B

$$H_1=\frac{1}{4}\left(\left(-P_1\lambda^4-P_2\lambda^2\beta^2-P_1\beta^4\right)\frac{(P_7\lambda^4+P_7\beta^4+P_8\lambda^2\beta^2)}{(P_5\lambda^4+P_5\beta^4+P_6\lambda^2\beta^2)}-k1-k2\left(\lambda^2+\beta^2\right)\right),$$

$$H_2=\frac{1}{4}\left(P_3\lambda^4+P_4\lambda^2\beta^2+P_3\beta^4\right),$$

$$H_3=-\left(\frac{(P_7\lambda^4+P_7\beta^4+P_8\lambda^2\beta^2)\lambda^2\beta^2}{P_5\lambda^4+P_5\beta^4+P_6\lambda^2\beta^2}\frac{8}{3}\frac{1}{mn\pi^2}\right),$$

$$H_4=-\left(\frac{P_1\lambda^2\beta^2}{P_5}\frac{4}{3mn\pi^2}\right),H_5=-\frac{1}{64P_5}\left(\lambda^4+\beta^4\right),H_6=\frac{4}{mn\pi^2},$$

$$P_1=\frac{-Q_2Q_3}{Q_1^2-Q_2^2}+\frac{Q_1Q_4}{Q_1^2-Q_2^2},\ P_2=\frac{2Q_1Q_3}{Q_1^2-Q_2^2}-\frac{2Q_2Q_4}{Q_1^2-Q_2^2}-\frac{2Q_{11}}{Q_6},$$

$$P_3=\frac{-Q_3(-Q_1Q_3+Q_2Q_4)}{Q_1^2-Q_2^2}-\frac{Q_4(-Q_1Q_4+Q_2Q_3)}{Q_1^2-Q_2^2}-Q_8,$$

$$P_4=\frac{-2Q_3(-Q_1Q_4+Q_2Q_3)}{Q_1^2-Q_2^2}-\frac{2Q_4(-Q_1Q_3+Q_2Q_4)}{Q_1^2-Q_2^2}-2Q_9+\frac{2Q_{11}Q_7}{Q_6}-2Q_{12},$$

$$P_5 = \frac{Q_1}{Q_1^2 - Q_2^2},\ P_6 = \frac{-2Q_2}{Q_1^2 - Q_2^2} + \frac{1}{Q_6},$$
$$P_7 = \frac{Q_1Q_4 - Q_2Q_3}{Q_1^2 - Q_2^2},\ P_8 = -\frac{2(-Q_1Q_3 + Q_2Q_4)}{Q_1^2 - Q_2^2} - \frac{Q_7}{Q_6}.$$

Appendix C

$$G_1 = \frac{4\left(P_5Q_3\lambda^6 + (P_5Q_4 - P_7 + P_6Q_3)\lambda^4\beta^2 + (P_5Q_3 + P_6Q_4 - P_8)\lambda^2\beta^4 + (P_5Q_4 - P_7)\beta^6\right)}{\pi^2 mn(\mathrm{P}_5\lambda^4 + P_5\beta^4 + P_6\lambda^2\beta^2)},$$
$$G_2 = \frac{\left(Q_1P_5\lambda^6 + Q_1P_5\lambda^2\beta^4 + P_6Q_2\lambda^2\beta^4 + Q_1P_6\lambda^4\beta^2 + P_5Q_2\lambda^4\beta^2 + P_5Q_2\beta^6\right)}{8(\mathrm{P}_5\lambda^4 + P_5\beta^4 + P_6\lambda^2\beta^2)},$$
$$G_3 = Q_5,$$
$$G_4 = \frac{4\left((P_5Q_4 - P_7)\lambda^6 + (P_5Q_3 - P_8 + P_6Q_4)\lambda^4\beta^2 + (P_5Q_4 + P_6Q_3 - P_7)\lambda^2\beta^4 + P_5Q_3\beta^6\right)}{(\mathrm{P}_5\lambda^4 + P_5\beta^4 + P_6\lambda^2\beta^2)\pi^2 mn},$$
$$G_5 = \frac{\left(P_5Q_2\lambda^6 + P_5Q_2\lambda^2\beta^4 + P_6Q_1\lambda^2\beta^4 + P_5Q_1\lambda^4\beta^2 + P_6Q_2\lambda^4\beta^2 + P_5Q_1\beta^6\right)}{8(\mathrm{P}_5\lambda^4 + P_5\beta^4 + P_6\lambda^2\beta^2)}.$$